Supporting Information

Photolysis of Gas-phase Atmospherically Relevant Monoterpene-derived Organic Nitrates

Yuchen Wang[†], Masayuki Takeuchi[‡], Siyuan Wang[#], Sergey A. Nizkorodov[&], Stefan France[§], Gamze Eris[†], Nga Lee Ng[*,†,¶,‡]

[†]School of Chemical and Bimolecular Engineering, Georgia Institute of Technology, Atlanta, Georgia 30332, USA

[‡] School of Civil and Environmental Engineering, Georgia Institute of Technology, Atlanta, Georgia 30332, USA

[&] Department of Chemistry, University of California, Irvine, California 92697, USA

[§] School of Chemistry and Biochemistry, Georgia Institute of Technology, Atlanta, Georgia 30332, USA

[#] Cooperative Institute for Research in Environmental Sciences (CIRES), University of Colorado, Boulder, CO and National Oceanic and Atmospheric Administration (NOAA), Chemical Sciences Laboratory (CSL), Boulder, CO

[¶]School of Earth and Atmospheric Sciences, Georgia Institute of Technology, Atlanta, Georgia 30332, USA

*Corresponding Author: Nga Lee Ng (ng@chbe.gatech.edu)

This supporting information contains 6 tables and 14 figures, totaling 30 pages including the cover page.

1. General procedure for the preparation of propylene-derived ONs
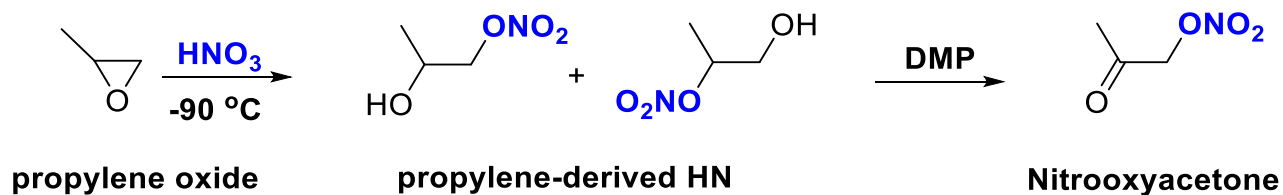
Scheme S1. The synthetic approach to synthesize propylene-derived ONs. DMP stands for Dess–Martin periodinane, which converts hydroxyl groups to carbonyl groups.

NMR spectra were recorded on a Bruker AV-400 spectrometer; chemical shifts were reported in parts per million (ppm) as values relative to the internal chloroform (7.27 ppm for ^{1}H and 77.23 ppm for ^{13}C). Abbreviations for signal coupling are as follows: s, singlet; d, doublet; t, triplet; q, quartet; m, multiplet.

Propylene-derived HN

Colorless liquid, 2.32 g, yield: 96%. ^{1}H NMR (400 MHz, CDCl$_3$) **δ** 5.20 (pd, J = 6.5, 3.4 Hz, 1H), 4.52 – 4.29 (m, 3H), 4.20 – 4.09 (m, 1H), 3.84 – 3.65 (m, 2H), 1.39 – 1.34 (m, 3H), 1.31 – 1.25 (m, 4H). ^{13}C NMR (101 MHz, CDCl$_3$) **δ** 81.40, 77.39, 64.43, 63.56, 19.08, 14.70.

Nitrooxyacetone

Colorless liquid, 0.27 g, yield: 36%. ^{1}H NMR (400 MHz, CDCl$_3$) **δ** 4.97 (s, 2H), 2.24 (s, 3H). ^{13}C NMR (101 MHz, CDCl$_3$) **δ** 199.23, 74.23, 25.98.

(a)

Propylene-derived HN

(b)

S3
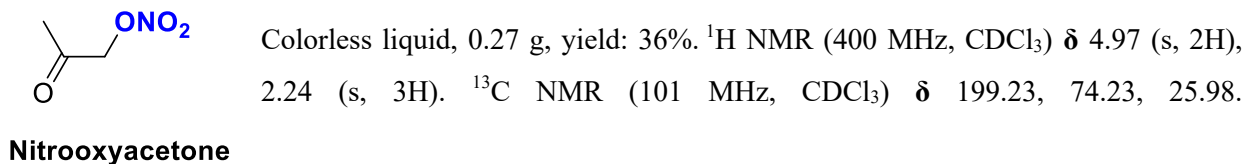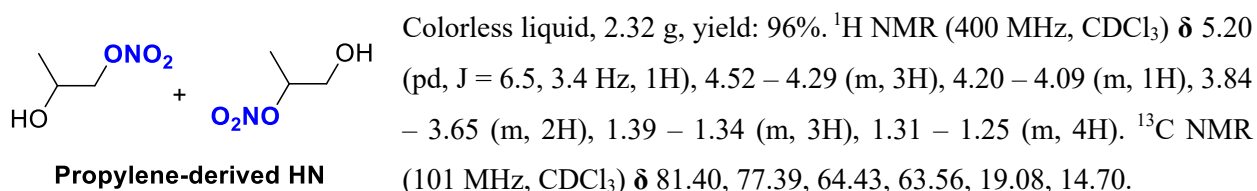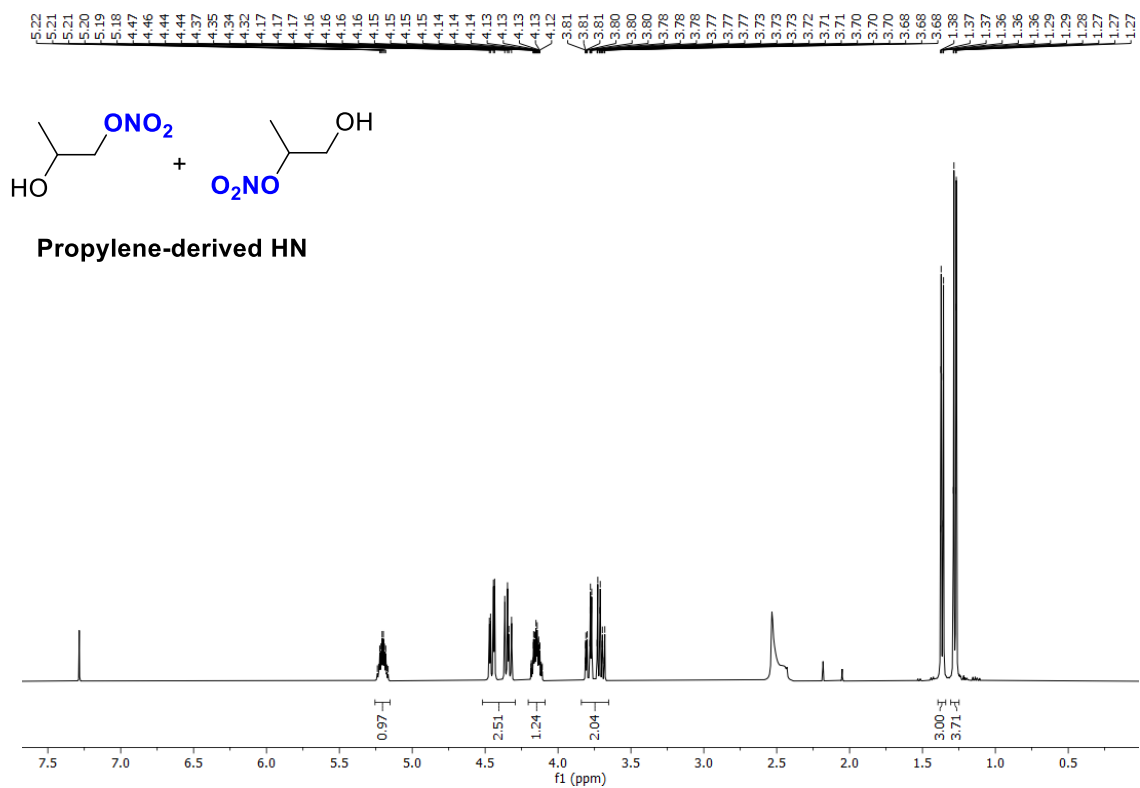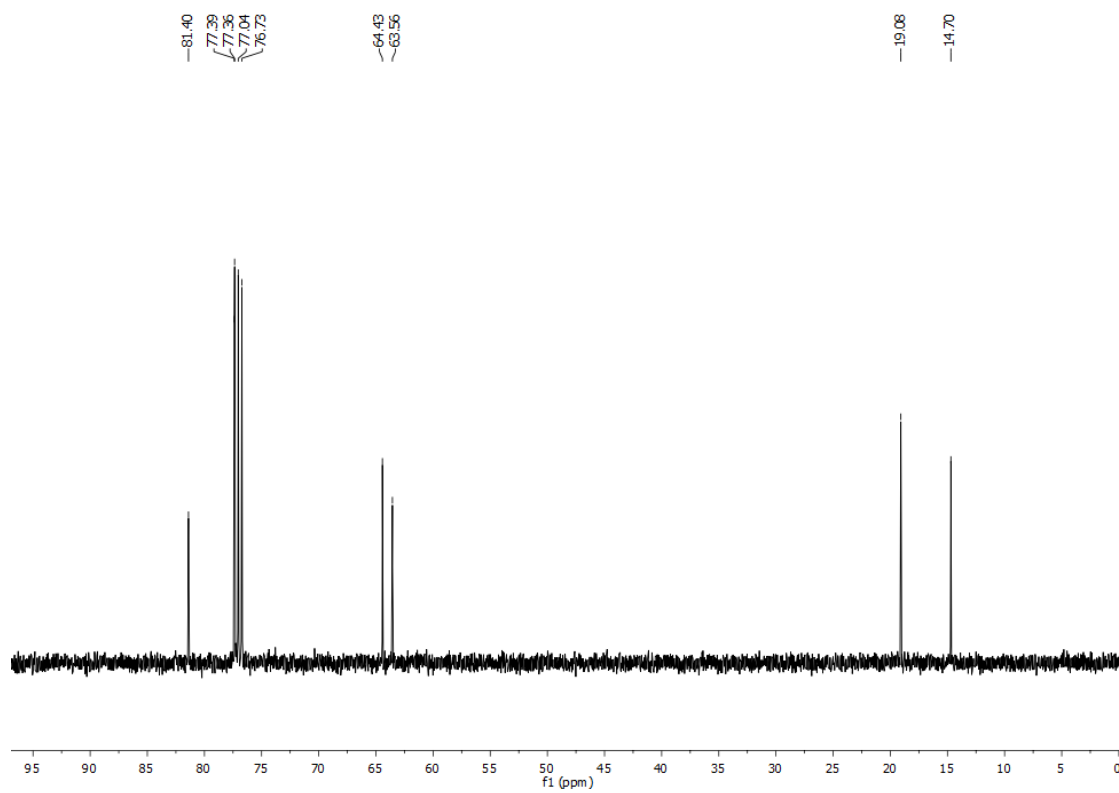
(c)
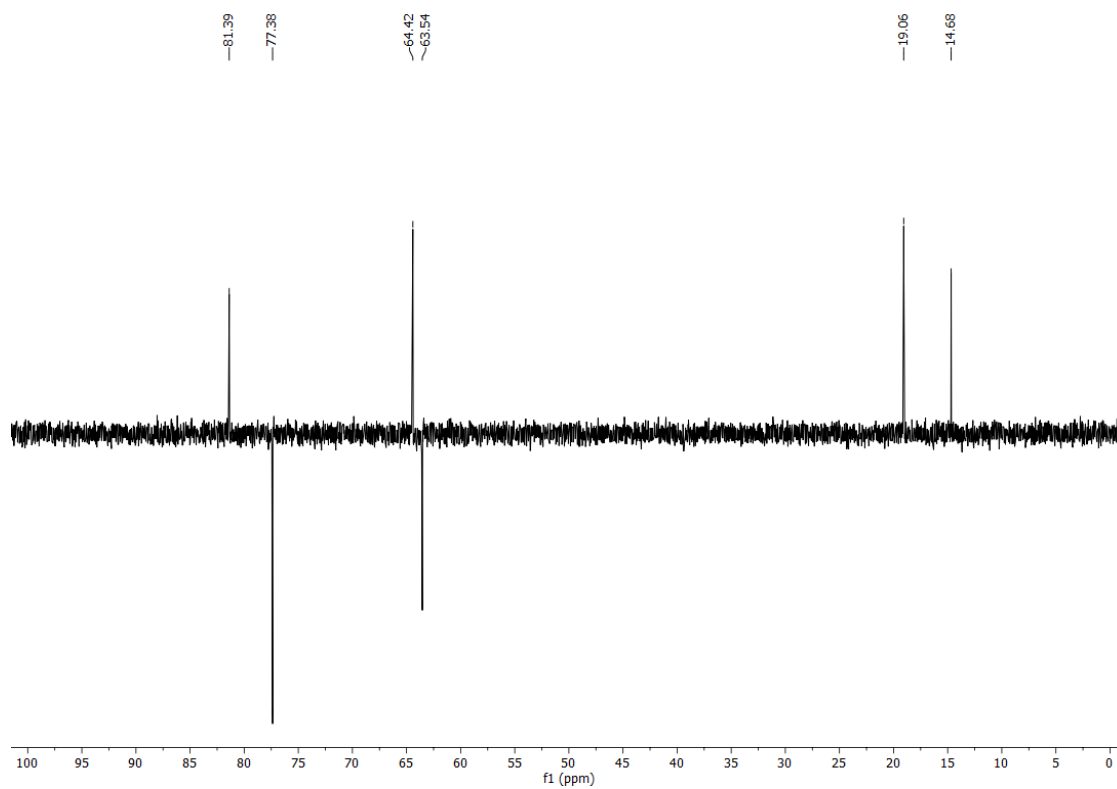
Figure S1. NMR spectra of propylene-derived HN isomers: (a) ^{1}H NMR, (b) ^{13}C NMR, and (c) DEPT-135.

(a)
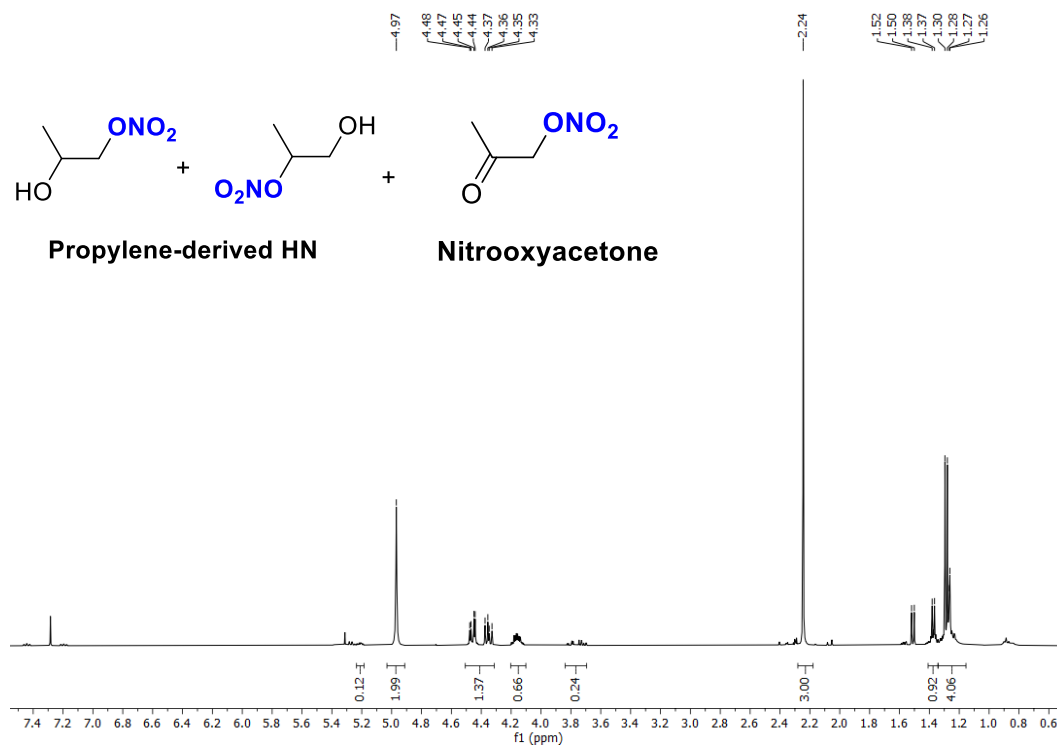
(b)
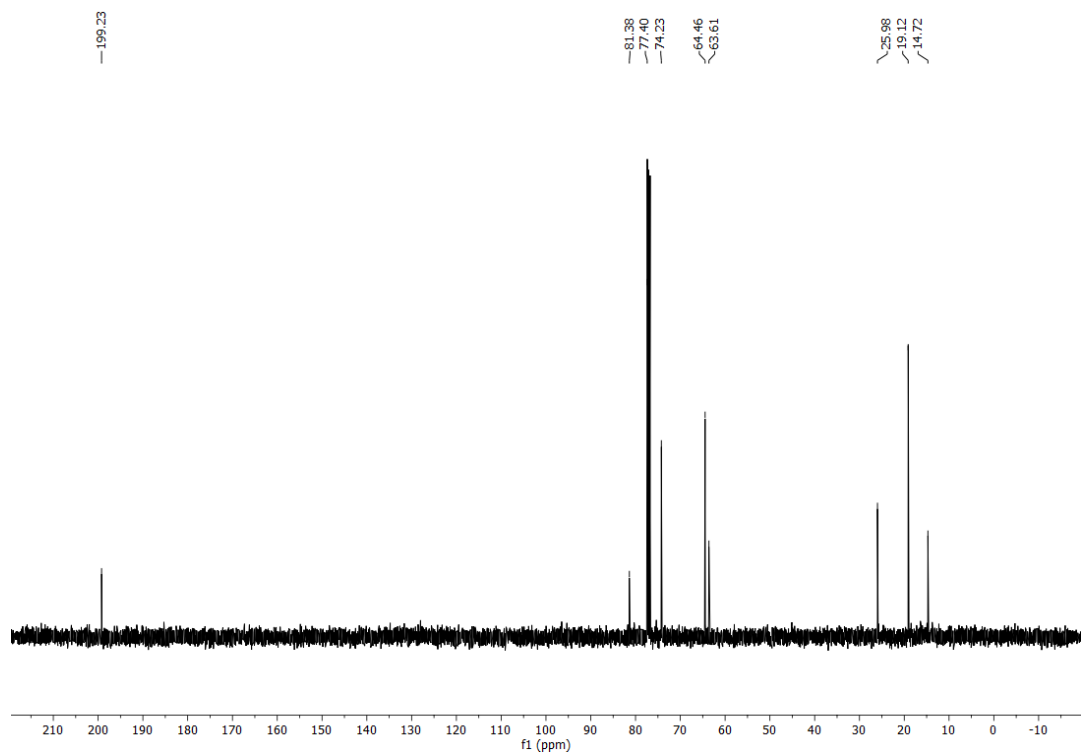
Figure S2. NMR spectra of the mixture of propylene-derived HN and nitrooxyacetone: (a) ^{1}H NMR and (b) ^{13}C NMR.

2. Photolysis of ONs in chamber experiments

During irradiation, in addition to photolysis, OH oxidation, ozonolysis, NO_3 radical reaction, and vapor wall loss can contribute to the decay of the MT-ON. The OH oxidation pathway was eliminated with cyclohexane added to the chamber as an OH scavenger (Table S2). We also ignored the NO_3 radical reaction during the irradiation period because of the negligible amount of NO_3 radicals, as detailed below. During photolysis experiments, the steady-state NO_3 concentrations were estimated to be in the range of $1.5-0.58\times10^{-2}$ pptv, based on the measured NO_2, O_3 and MT-ON concentrations. The characteristic time scales of NO_3 production (~43 s) and N_2O_5 decomposition (~33 s) estimated by NO_2, O_3 and MT-ON concentrations implied that $NO_2/NO_3/N_2O_5$ can reach equilibrium in a minute in the chamber. Therefore, the estimated steady-state NO_3 concentrations were the upper limits of NO_3 concentrations in the chamber. There is no previous work that reports the NO_3 reaction rate constant of MT-ONs. Thus, we employed the NO_3 reaction rate constant of monoterpenes (*i.e.*, α-pinene, limonene, and β-pinene, MCM version 3.3.1) to estimate the NO_3 reaction lifetimes of the corresponding MT-ONs in the chamber. The NO_3 reaction lifetimes were estimated to be 202 h, 158 h, and 291 h for 3º_ApHN, 2º_LmHN, and 1º_BpHN, respectively.

The ozonolysis rate constants of MT-ONs were determined from separate ozonolysis experiments. In these experiments, MT-ON (*i.e.*, 3º_ApHN, 2º_LmHN, or 1º_BpHN, <10 ppbv) and cyclohexane (10 ppmv) were injected into the chamber, following the same protocol as in the photolysis experiments. Excess O_3 (~110 ppbv) was used so that the decay of MT-ON can be treated as pseudo first-order. The O_3 concentration during the experiment was continuously monitored by O_3 monitor. We calculated the MT-ON ozonolysis rate constant by fitting the natural log of normalized $C_{10}H_{17}NO_4I^-$ signal versus the time integration of O_3 concentration. The ozonolysis rate constants of MT-ONs (k_{O3}) are summarized in Table S2.

The vapor wall loss rate constant (k_{vwl}) of each photolysis experiment was set to be the average of k_{D1} and k_{D3} (Table S1 and section S3), in which k_{D1} and k_{D3} are the vapor wall loss rate constants in **D1** and **D3** periods (before and after irradiation), respectively.

We used a novel regression approach to determine the photolysis rate constants ($J_{chamber}$). The prognostic equation of the decay of MT-ON in the chamber can be approximated by:

$$\frac{d[MT\_ON]}{dt} = -(J_{chamber} + k_{vwl})[MT\_ON] - k_{O_3}[MT\_ON][O_3] \tag{S1}$$

Where [MT-ON] and $[O_3]$ are the concentrations of MT-ON and O_3 (both in molecule cm^{-3}), respectively. k_{vwl} (s^{-1}) is the vapor wall loss rate constant, and k_{O3} (cm^3 molecule^{-1} s^{-1}) is the ozonolysis rate constant.

Integrating this differential equation gives the analytical solution:

$$MT\_ON(t) = MT\_ON(0) * \exp\left[-(J_{chamber} + k_{vwl})t - k_{O_3}\int_{t=0}^{t} O_3(t)dt\right]$$

(S2)

Where MT-ON(t) and O_3(t) are MT-ON and O_3 concentrations as function of time; MT-ON(0) is the initial concentration of MT-ON (*i.e.*, concentration at t=0 s). The $k_{O_3}\int_{t=0}^{t} O_3(t)dt$ term is the ozone integral over time, which can be derived by integrating the observed ozone time series during the irradiation stage of each experiment. Equation S2 is then be fitted to the observed MT-ON time series to determine the optimized $J_{chamber}$. The total uncertainty of $J_{chamber}$ is estimated using 95% confidence interval (2 standard deviations) from the fitting propagated with uncertainties from k_{vwl} and k_{O3}.

The robustness of this fitting approach is supported by two additional exercises: (a) when plugging the resulting $J_{chamber}$ into the box model, the simulated time series of MT-ON is nearly identical to that calculated using Equation S2, also in excellent agreement with observations (Figure S3, 3°_ApHN in experiment 2 as an example). This is not surprising since the box model is essentially solving the initial value problem defined by Equation S1. (b) when setting $J_{chamber}$ to zero and fitting Equation (S2) to the measurements collected during **D2**, the resulting k_{O3} is consistent with k_{O3} derived from the separate ozonolysis experiments with respect to uncertainties.
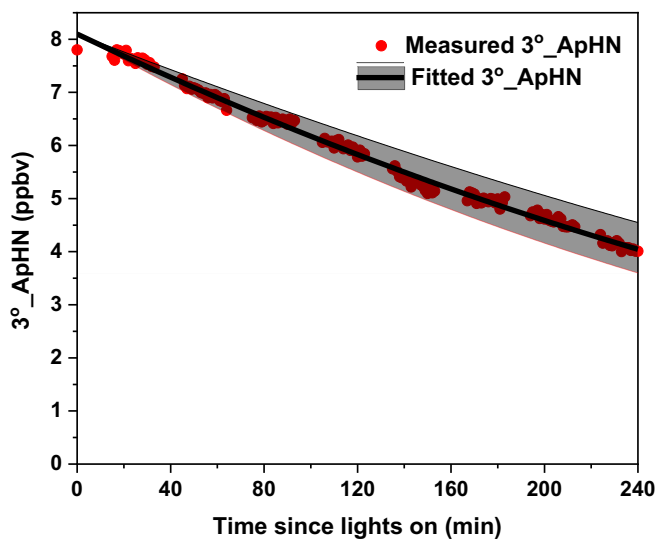
Figure S3. Time series of fitted and measured 3°_ApHN (Experiment 2 in Table S1) during irradiation period.

Table S1. The rate constants of ONs determined for each period during experiment.

ONs	Structures	Exp.	k_{D1} $(\times 10^{-5}\ s^{-1})^a$	k_{UV} $(\times 10^{-5}\ s^{-1})^a$	k_{D2} $(\times 10^{-5}\ s^{-1})^a$	k_{D3} $(\times 10^{-5}\ s^{-1})^a$	k_{vwl} $(\times 10^{-5}\ s^{-1})^{a,e}$
Nitrooxyacetone		1	0.83 ± 0.093	0.98 ± 0.015	0.65 ± 0.081	0.65 ± 0.081	0.74 ± 0.087^d
		2	0.47 ± 0.12	0.52 ± 0.077	0.26 ± 0.037	0.26 ± 0.037	0.37 ± 0.079^d
3°_ApHN		1	$/^b$	5.0 ± 0.21	3.2 ± 0.60	2.9 ± 0.84	2.9 ± 0.84
		2	2.2 ± 1.0	4.4 ± 0.080	2.5 ± 0.80	2.0 ± 0.36	2.1 ± 0.70
		3^c	n/a	n/a	n/a	n/a	1.9 ± 0.012
2°_LmHN		1	0.88 ± 0.52	2.4 ± 0.047	0.93 ± 0.12	$/$	0.88 ± 0.52
		2	0.95 ± 0.062	2.3 ± 0.026	1.2 ± 0.082	0.66 ± 0.28	0.81 ± 0.17
		3^c	n/a	n/a	n/a	n/a	0.88 ± 0.020
1°_BpHN		1	1.08 ± 0.067	1.8 ± 0.072	1.4 ± 0.40	$/$	1.08 ± 0.067
		2	1.7 ± 0.28	2.1 ± 0.057	1.7 ± 0.15	1.6 ± 0.16	1.6 ± 0.22
		3^c	n/a	n/a	n/a	n/a	1.5 ± 0.016
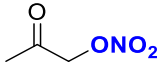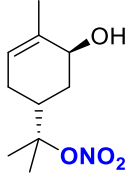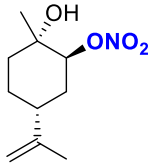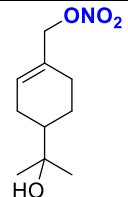
[a.] The uncertainties correspond to the uncertainties of linear fitting (2 standard deviations); [b.] Data not available due to HR-ToF-CIMS instrumental problem; [c.] Separate vapor wall loss experiments; [d.] Nitrooxyacetone does not react with ozone. Therefore, k_{D2} equals to k_{D3} for nitrooxyacetone. [e.] Vapor wall loss rate constants in photolysis experiments for MT-ONs $= (k_{D1} + k_{D3})/2$.

Table S2. Summary of photolysis rate constants of MT-ONs and scavenging efficiency of OH scavenger in this work.

Compounds	k_{O3} ($\times 10^{-17}$ cm^3 molecule^{-1} s^{-1})	Exp.	Concentration (ppbv)[a]	$J_{chamber}$ ($\times 10^{-5}$ s^{-1})	$\tau_{chamber}$ (h)[e]	k_{OH} ($\times 10^{-11}$ cm^3 molecule^{-1} s^{-1})[f]	Scavenging efficiency[g]	Photolysis fraction[h]
Nitrooxyacetone	/	1	20.4	0.33 ± 0.10[c]	84 ± 26	0.07	100%	100%
		2	/[b]	0.26 ± 0.11[c]	108 ± 46		/[b]	/[b]
		Average	/	$\mathbf{0.29 \pm 0.11}$[d]	$\mathbf{95 \pm 36}$		100%	100%
3°_ApHN	4.2 ± 0.60	1	6.3	2.4 ± 0.80[i]	12 ± 4.0	9.9	98.8%	97.2%
		2	7.8	2.2 ± 0.80[i]	13 ± 4.7		98.9%	97.2%
		Average	/	$\mathbf{2.3 \pm 0.80}$[d]	$\mathbf{12 \pm 4.2}$		**98.9%**	**97.2%**
2°_LmHN	1.7 ± 0.16	1	3.7	1.2 ± 0.70[i]	23 ± 13	5.9	99.7%	99.2%
		2	5.3	1.4 ± 0.30[i]	20 ± 4.3		99.6%	99.0%
		Average	/	$\mathbf{1.3 \pm 0.50}$[d]	$\mathbf{21 \pm 8.1}$		**99.6%**	**99.1%**
1°_BpHN	1.1 ± 0.13	1	2.7	0.50 ± 0.10[i]	56 ± 11	5.7	99.7%	98.0%
		2	7.7	0.60 ± 0.10[i]	46 ± 7.7		99.2%	97.3%
		Average	/	$\mathbf{0.55 \pm 0.10}$[d]	$\mathbf{51 \pm 9.3}$		**99.5%**	**97.7%**

a. Measured by TD-CAPS; b. Data not available due to TD-CAPS instrumental problem; c. The uncertainties were calculated by propagation of statistical errors associated with rate constants for the dark (k_{D2}) and irradiation periods (k_{UV}); d. The uncertainties were propagated from the statistical errors associated with the average of uncertainties of two duplicate photolysis experiments; e. The uncertainties were propagated from the uncertainties of $J_{chamber}$; f. Estimated k_{OH} from Master Chemical Mechanism (version 3.3.1) or Estimation Program interface Suite (EPI Suite[TM], https://www.epa.gov/tsca-screening-tools/epi-suitetm-estimation-program-interface); g. Cyclohexane concentration was 10 ppmv. The reaction rate constant of OH and cyclohexane is 7.1×10^{-12} cm^3 molecule^{-1} s^{-1} (Master Chemical Mechanism, version 3.3.1); h. The background OH concentration in chamber was 5.8×10^5 molecule cm^{-3} (determined from separate background experiments with cyclohexane as OH tracer). Photolysis to photooxidation ratio = ($J_{chamber}$) /($J_{chamber}$ + [OH] $\times k_{OH} \times$ (1-scavenging efficiency)); i. The uncertainties were propagated from the statistical errors associated with k_{vwl} and k_{O3}.

Table S3. Photolysis measurements reported in this study and in the literature.[1–6]

Literature	Solar spectra	Organic nitrates	Photolysis rate constant ($\times 10^{-5}$ s^{-1})	Photolysis lifetime (h)
Barnes et al., 1993[1][a]	0 ° zenith angle	1,2-Propandiol dinitrate	1.1	26
		1,2-Butandiol dinitrate	1.4	20
		2,3-Butandiol dinitrate	1.1	26
		3,4-Dinitrooxy- 1-butene	0.63	44
		1,4-Dinitrooxy-2-butene	0.63	44
		Nitrooxyacetone	3.5	7.8
		1-Nitrooxy-2-butanone	2.1	13
		3-Nitrooxy-2-butanone	5.4	5.2
Treve and Rudich, 2003[2][a]	30° N, summer	C3-C6 hydroxyalkyl nitrates	0.10	277
Suarez-Bertoa et al., 2012[3][b]	1 July at noon at 40° N	**Nitrooxyacetone**	4.8	5.8
		3-nitrooxy-2-butanone	5.7	4.9
		3-methyl-3-nitooxy-2-butanone	7.4	3.8
Müller et al., 2014[4][a]	30 ° zenith angle	**Nitrooxyacetone**	3.5	7.9
		1-hydroxy-3-oxobutan-2-yl nitrate	5.6	5.0
		2-hydroxy-3-oxobutyl nitrate	3.2	8.7
		2-oxoethyl nitrate	15	1.9
		1-hydroxy-2-methyl-3-oxopropan-2-yl nitrate	35	0.80
		4,1-isoprene nitrooxy enal	56	0.50
Xiong et al, 2016[5][b]	45 ° zenith angle	4,1-isoprene nitrooxy enal	31	0.90
Picquet-Varrault et al., 2020[6][b]	1 July at noon at 40° N	4-nitrooxy-2-butanone	6.1	4.6
		5-nitrooxy-2-pentanone	3.3	8.4
This work[b]	28 ° zenith angle	**Nitrooxyacetone**	1.7	16
		3º_ApHN	8.3 – 14	2.0 – 3.3
		2º_LmHN	3.0 – 8.1	3.4 – 9.2
		1º_BpHN	1.7 – 4.1	6.8 – 17

[a.] Theoretical calculations of photolysis rate constants based on previously reported or measured absorption cross sections of organic nitrates and solar spectra; [b.] Chamber photolysis rate constants of organic nitrates; reference compounds (*e.g.*, NO_2) used to convert chamber photolysis rate constants under chamber lights to ambient photolysis rate constants under solar spectra.
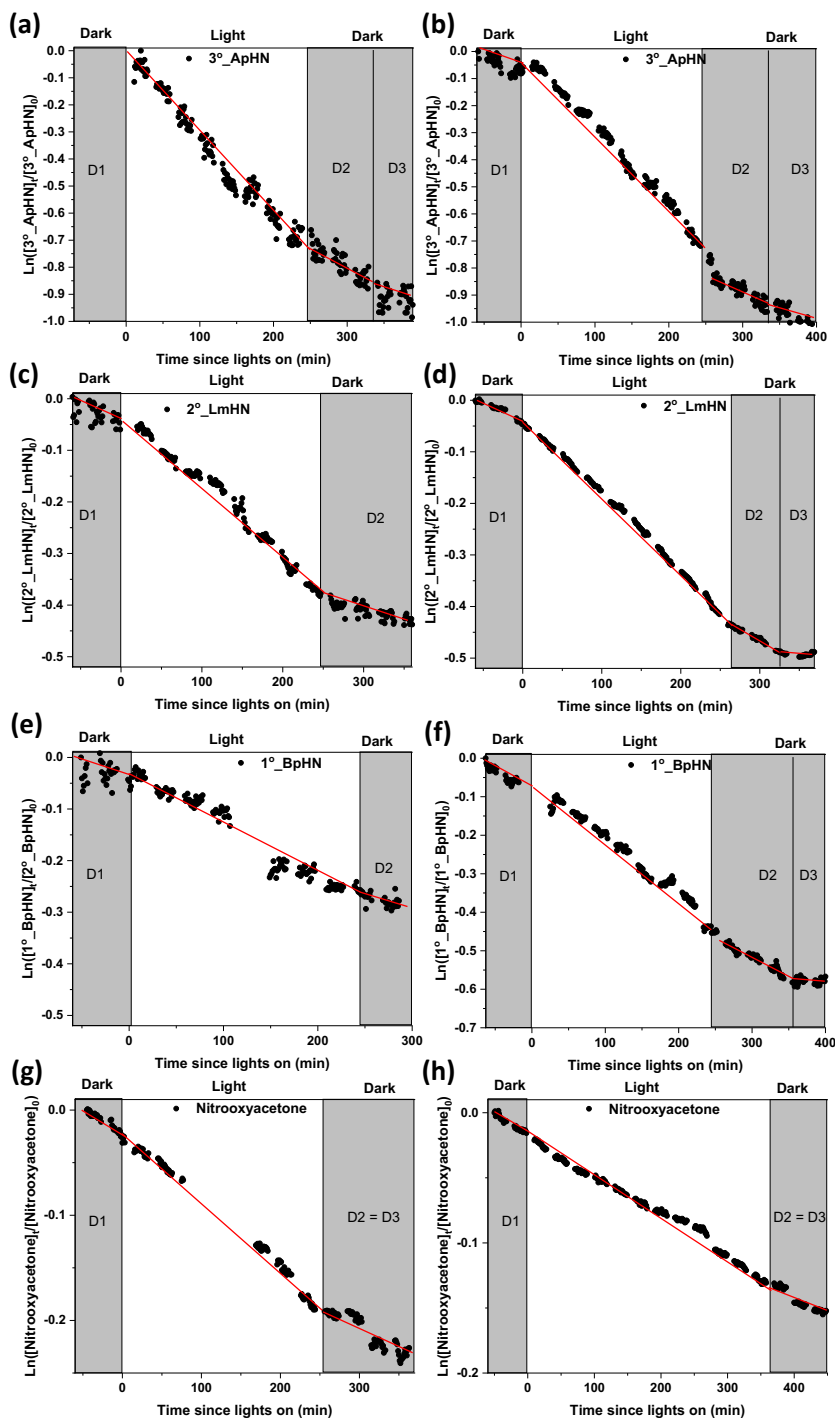
Figure S4. First-order kinetics analysis for photolysis of (a), (b) 3°_ApHN in experiments 1 and 2; (c), (d) 2°_LmHN in experiments 1 and 2; (e), (f) 1°_BpHN in experiments 1 and 2; and (g), (h) Nitrooxyacetone in experiments 1 and 2. The red line in each period corresponds to first-order kinetics-fitting curve. D1 is the dark period before irradiation time (lights on). **D2** and **D3** are dark periods after irradiation time. Detailed discussion for each period is provided in section 2.2 in the main text. Nitrooxyacetone does not react with O_3. Therefore, k_{D2} equals to k_{D3} for nitrooxyacetone.
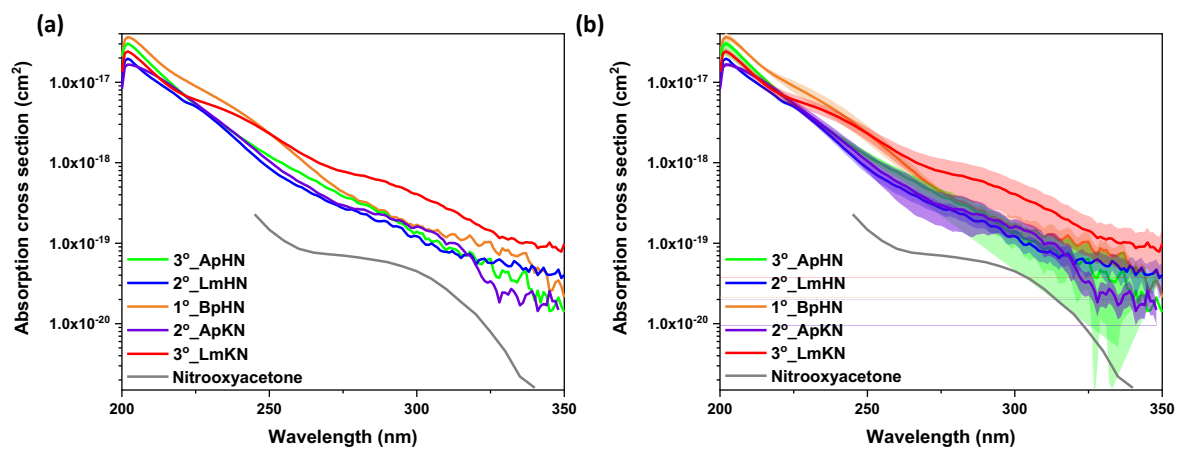
Figure S5. (a) Absorption cross sections for MT-ONs and nitrooxyacetone. The absorption cross sections for MT-ONs were measured in ethyl ether in this study. The absorption cross section of nitrooxyacetone is extracted from Roberts and Fajer, 1989[7] and Barnes et al., 1993.[1] (b) Absorption cross sections for MT-ONs and nitrooxyacetone with uncertainties. The uncertainties in the shaded areas were from the average of measured absorption cross sections in different solution concentrations.

Table S4. Estimated ambient photolysis rate constants and lifetimes for 2º_ApKN and 3º_LmKN.
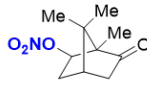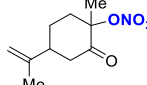
	2º_ApKN	3º_LmKN
Structures		
Cutoff wavelength (nm)	312	
$J_{ambient}$ (×10^{-5} s^{-1})	3.6	9.0
$\tau_{ambient}$ (h)	7.9	3.1
Cutoff wavelength (nm)	330	
$J_{ambient}$ (×10^{-5} s^{-1})	12	40
$\tau_{ambient}$ (h)	2.3	0.69

3. Vapor wall loss measurements of MT-ONs

In addition to measuring vapor wall loss of 3º_ApHN, 2º_LmHN, and 1º_BpHN in photolysis experiments, we also measured them as k_{vwl} in separate vapor wall loss experiments (Experiments 3 in Table S1). In these experiments, we observed a fast initial decay and a deceleration afterwards for 2º_LmHN and 1º_BpHN, but 3º_ApHN exhibited a constant decay rate throughout the experiment (Figure S6). According to the two-layer model in Huang et al.,[8] the vapor wall loss process can be considered in three stages. The first stage is vapor molecules traversing a gas-phase boundary layer which is negligible (< 10 s). Then, the vapor molecules undergo adsorption and desorption at the outer polymer layer of the chamber wall (surface layer). In the second stage, the initial decay of vapor is fast (adsorption dominated), which then gradually slows down and reaches an equilibrium between adsorption and desorption. Simultaneously, the adsorbed vapor molecules can slowly diffuse into the interior of the polymer film of the chamber wall (inner layer). The vapor wall loss rate constant is the overall decay of vapor molecules in the surface and inner layers after the equilibrium, which is observed to have first-order kinetics. In this work, we followed the two-layer model in Huang et al.[8] and defined the first-order decay of vapor molecules after the equilibrium as the measured k_{vwl}. The initially fast decays of 2º_LmHN and 1º_BpHN were presumably dominated by their adsorption onto the chamber wall. The equilibrium lifetimes for 2º_LmHN and 1º_BpHN were 55 and 75 min, respectively (Figure S7 and SI section 3.2). The degradation of 2º_LmHN and 1º_BpHN during the deceleration period (after equilibrium) versus time can be fitted by first-order decay rate, which was defined as measured k_{vwl}. The k_{vwl} for 2º_LmHN was 0.88×10^{-5} s^{-1} and for 1º_BpHN was 1.5×10^{-5} s^{-1} (Table S5). Different from 2º_LmHN and 1º_BpHN, we observed a constant decay rate for 3º_ApHN, which we speculated the equilibrium of adsorption and desorption of 3º_ApHN to the chamber wall was reached during the one hour of injection. The k_{vwl} for 3º_ApHN was determined to be 1.9×10^{-5} s^{-1}. In photolysis experiments, although the vapor wall loss could not reach equilibrium for 2º_LmHN (injection time: 20 min) and 1º_BpHN (injection time: 1 h) during injection, it could reach equilibrium during the **D1** period. For 3º_ApHN, the adsorption and desorption to chamber wall could reach equilibrium during injection (injection time: 1 h). Therefore, both k_{D1} and k_{D3} in photolysis experiments correspond to vapor wall loss rate constants of MT-ONs and their average was used in subsequent discussions. When comparing vapor wall loss rate constants in photolysis experiments and vapor wall loss experiments, they are in general agreement with up to 52% difference.

Accounting for vapor wall loss is important to obtain accurate secondary organic aerosol (SOA) yields in chamber experiments.[9–16] Therefore, we compared the measured k_{vwl} to theoretical calculation of k_{vwl}. Based on the chemical structures of MT-ONs used in this work, we evaluated different methods in literature[8,14,15,17] (Table S5) to obtain theoretical vapor wall loss and equilibrium lifetimes. Using the two-

layer model in Huang et al.,[8] the theoretical k_{vwl} for 3°_ApHN, 2°_LmHN, and 1°_BpHN were determined to be 1.01×10^{-5} s^{-1}, 9.4×10^{-6} s^{-1}, and 8.4×10^{-6} s^{-1}, respectively. These theoretical k_{vwl} values were in the same order of magnitude as the measured k_{vwl} in this work with a discrepancy of 7-47%. The discrepancy was mainly from the equation used to calculate the relative inner layer mass transport rate constant, as the uncertainty of each parameter in the equation is around 60-70% (Figure S8). The theoretical equilibrium lifetimes for these MT-ONs ranged from 36-52 min. In addition, Zhang et al.,[14,15] reported empirical equations to estimate vapor wall loss and equilibrium lifetimes of MT-ONs based on experimental data. When applying the equations reported in Zhang et al.,[14,15] the theoretical k_{vwl} for 3°_ApHN, 2°_LmHN, and 1°_BpHN were found to be 1.2×10^{-5} s^{-1}, 1.1×10^{-5} s^{-1}, and 9.6×10^{-6} s^{-1}, respectively. The discrepancy with our measured k_{vwl} was 24-36%. The theoretical equilibrium lifetimes estimated by the equations reported in Zhang et al.[14,15] were 23-29 h, which were much longer than our observation.

3.1 First-order kinetics analysis for vapor wall loss of MT-ONs
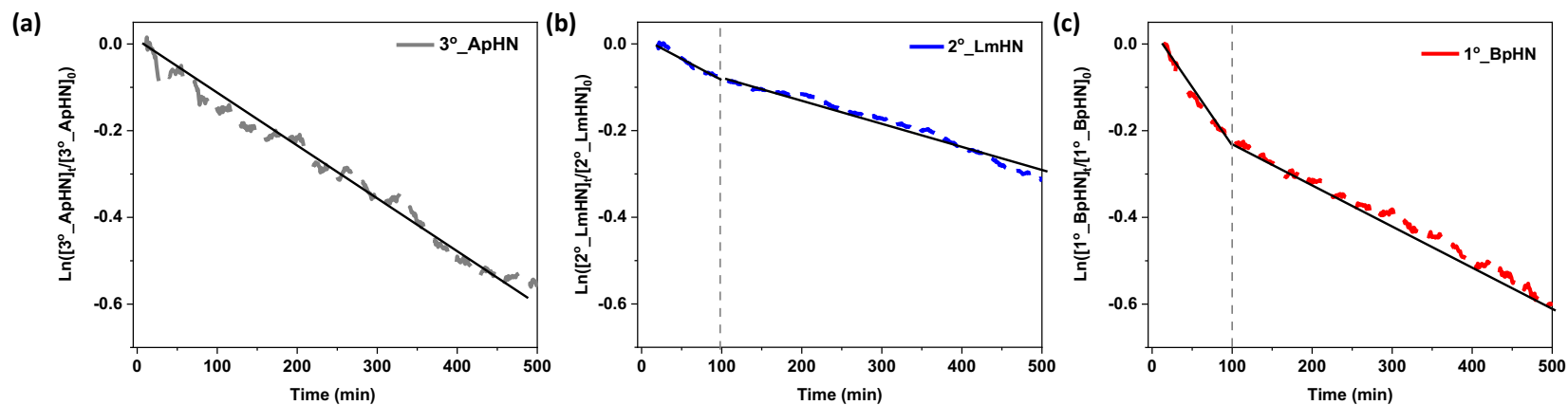
Figure S6. First-order kinetics analysis for vapor wall loss of (a) 3°_ApHN; (b) 2°_LmHN; and (c) 1°_BpHN. The black line in each figure is the first-order kinetics fitting line. The grey dash line in figures S5b and S5c indicates the time change from the fast initial decay to the deceleration afterwards for 2°_LmHN and 1°_BpHN.

3.2 Vapor wall loss equilibrium lifetimes for 2°_LmHN and 1°_BpHN

The time scales for reaching gas-wall partitioning equilibrium of 2°_LmHN and 1°_BpHN were determined by fitting the data to the exponential equation, which was reported in Krechmer et al.[17]:

$$y(t) = y_E + (y_0 - y_E)\exp\left(-\frac{t-t_0}{\tau_E}\right)$$ (S3)

In this equation, t_0 is the time of the peak MT-ON concentration y_0, y_E is the equilibrium concentration, and τ_E is the equilibrium lifetime.

In vapor wall loss experiments, we observed a fast initial decay and a deceleration afterwards for 2°_LmHN and 1°_BpHN, but 3°_ApHN exhibited a constant decay rate throughout the experiment (Figure S6). According to Figures S5b and S5c, the decay rates of 2°_LmHN and 1°_BpHN changed at 100 min. The times series of 1°_BpHN and 2°_LmHN before that time were shown in Figure S7. By employing Equation S3, the equilibrium lifetimes for 1°_BpHN and 2°_LmHN were determined to be 75 and 55 min, respectively.
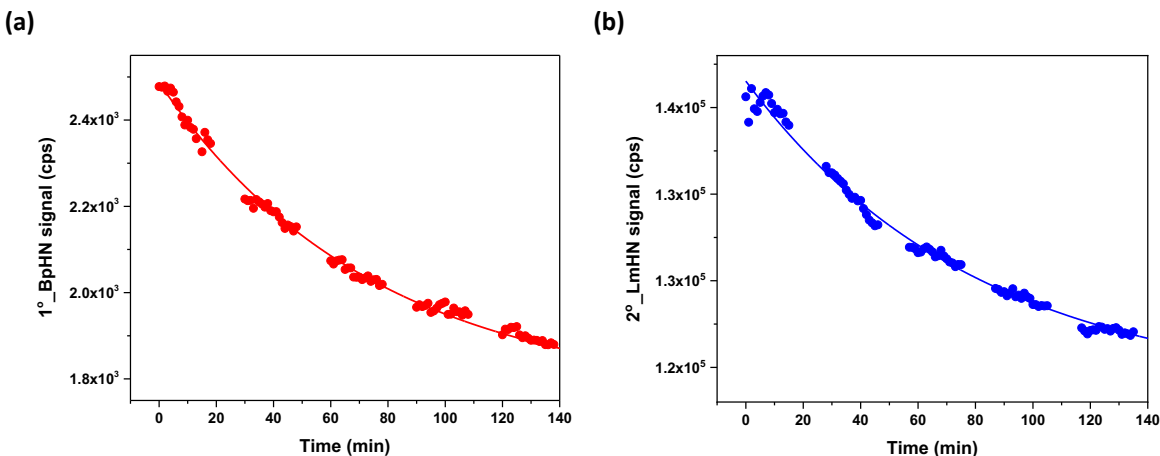
Figure S7. Time series of 1°_BpHN and 2°_LmHN before gas-wall partitioning equilibrium. The solid line in each figure is the fitting curve by Equation S3.

3.3 Comparison of measured and theoretical k_{vwl}

Table S5. Comparison of measured vapor wall loss rate constants in this work and theoretical vapor wall loss rate constants determined based on formulations reported in previous work.[8,14]

Compounds	Structures	Measured k_{vwl} $(\times 10^{-5}\ s^{-1})^a$	c* $(\mu g\ m^{-3})^b$	Theoretical k_{vwl} $(\times 10^{-5}\ s^{-1})$ Huang et al., 2018	Difference between measured and theoretical k_{vwl}	Theoretical k_{vwl} $(\times 10^{-5}\ s^{-1})$ Zhang et al., 2015	Difference between measured and theoretical k_{vwl}
3°_ApHN		1.9 ± 0.012	2375.6	1.01	47%	1.2	36%
2°_LmHN		0.88 ± 0.020	4007.3	0.94	7%	1.09	24%
1°_BpHN		1.51 ± 0.016	7834.5	0.84	44%	0.96	36%
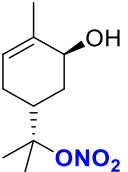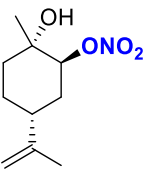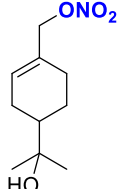
a. The uncertainties correspond to the uncertainties of linear fitting (2 standard deviations); b. c* is the vapor saturation concentration. c* is calculated from saturated vapor pressure estimated by EVAPORATION model[18].
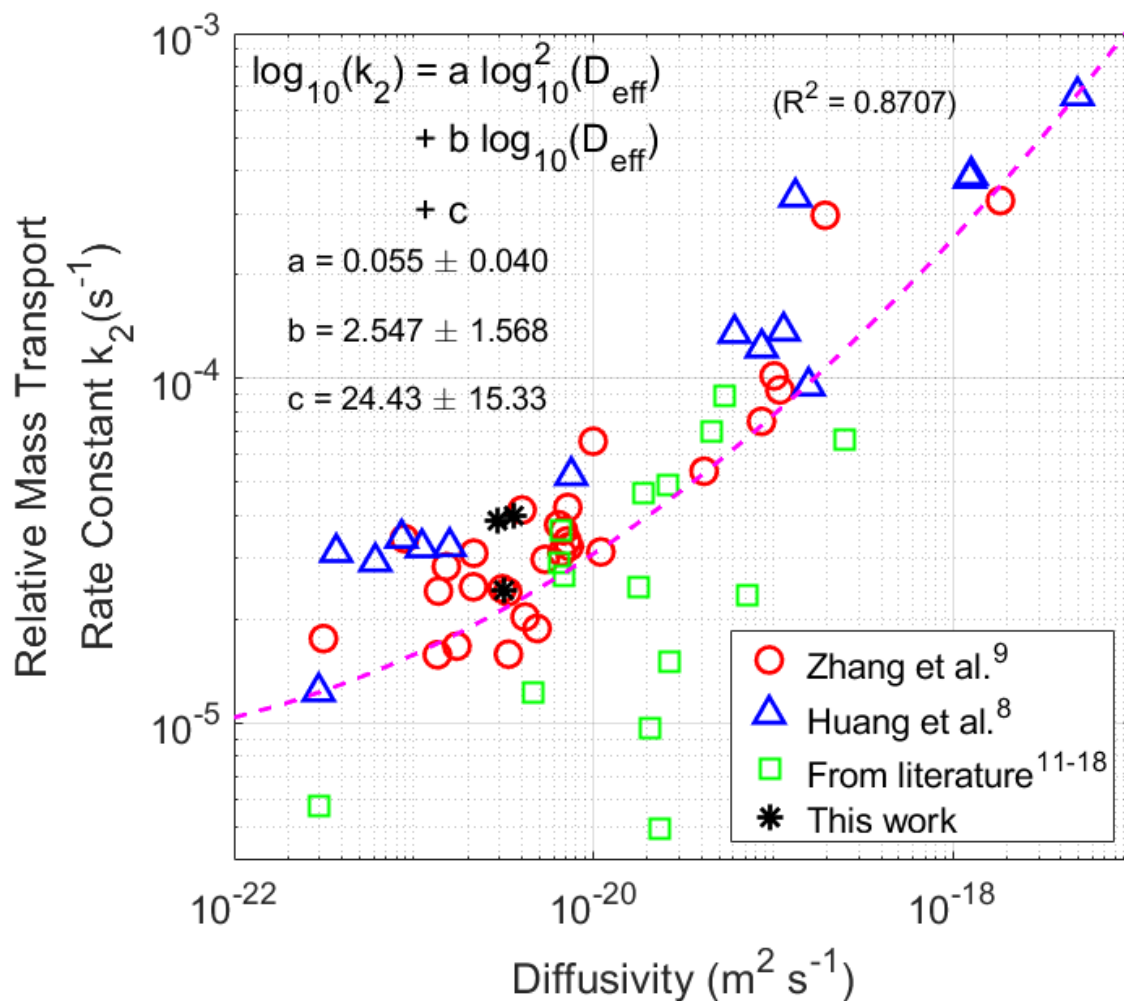
Figure S8. Empirical relationship between compound molecular diffusivity (m^2 s^{-1}) and relative inner layer mass transport rate constant k_2 (s^{-1}). Modified from Figure 5 in Huang et al[8] and the references therein.[14,19-26] Reproduced with permission from Huang et al[8], Copyright 2018, *Environ. Sci. Technol*.

4. Major photolysis products and proposed photolysis mechanisms
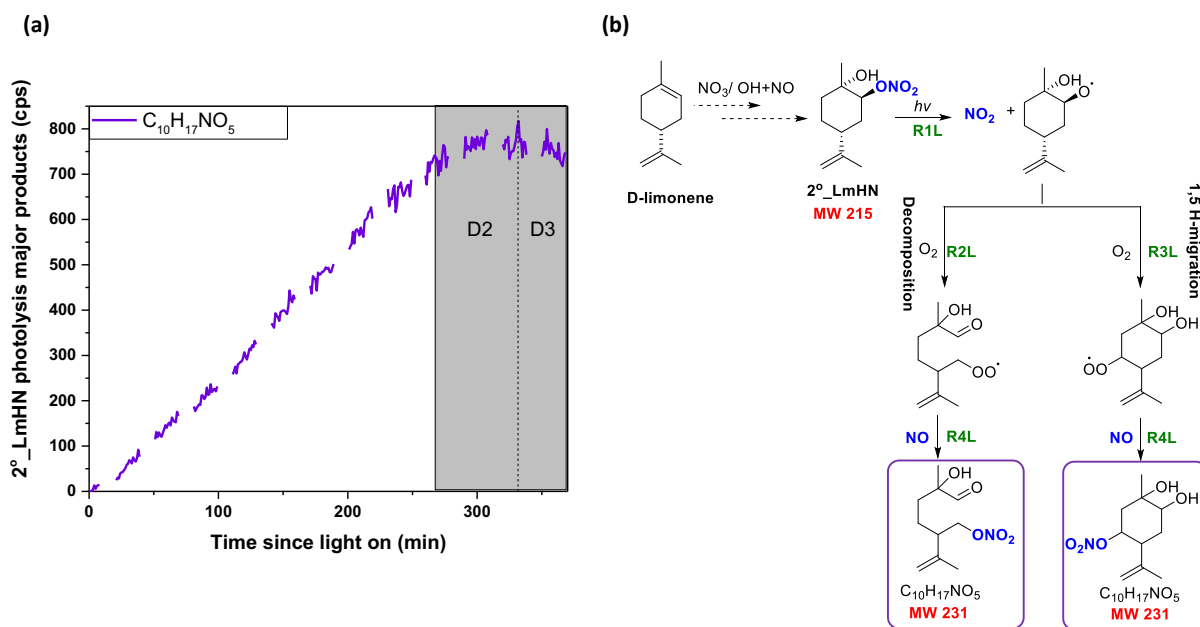
Figure S9. (a) Time series of major gas-phase product ($C_{10}H_{17}NO_5$) from photolysis of 2^o_LmHN measured by the HR-ToF-CIMS. D2 and D3 are dark periods after irradiation time. Detailed discussion for each period is provided in sections 2.2 in main text; (b) Proposed formation mechanism of $C_{10}H_{17}NO_5$ during 2^o_LmHN photolysis experiment. $C_{10}H_{17}NO_5$ was identified by HR-ToF-CIMS (boxed).
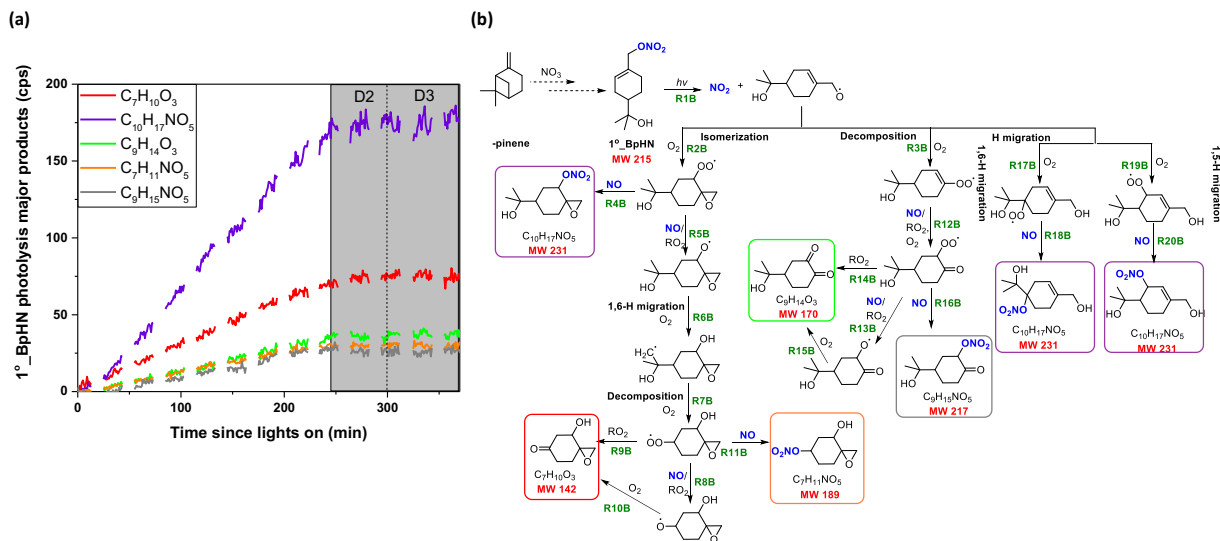
Figure S10. (a) Time series of major gas-phase products from photolysis of 1°_BpHN measured by the HR-ToF-CIMS. D2 and D3 are dark periods after irradiation time. Detailed discussion for each period is provided in sections 2.2 in main text; (b) Proposed formation mechanism of major gas-phase products during 1°_BpHN photolysis experiment. The compounds in the boxes were major gas-phase products identified by HR-ToF-CIMS.

Figure S11. Proposed mechanism and estimated rate constants (by structure–activity relationships [27,28] or Master Chemical Mechanism, version 3.3.1[29–31]) of photolysis of 3°_ApHN. The compounds in blue boxes were identified by HR-ToF-CIMS. The reactions reported in Master Chemical Mechanism (MCM, version 3.3.1) were highlighted in green.

5. Box-model simulations of 3º_ApHN photolysis

5.1 Measurement of photolysis rate constant of NO_2 in chamber

122 ppbv of NO_2 from a cylinder containing 500 ppmv of NO_2 (Matheson) was injected into the chamber at 5 L min^{-1} and kept in the dark for 20 min. The lights were turned on for 20 min. 96 ppbv of NO_2 underwent photolysis to produce 20 ppbv NO and 21 ppbv of O_3. The photolysis rate constant for NO_2 (J_{NO2}) was subsequently determined to be 2.1×10^{-3} s^{-1} by a kinetic model.

5.2 The organic and inorganic reactions involved in this work

In this work, we included both organic and inorganic reactions in model simulations. The organic reactions reported in MCM were highlighted in green in Figure S11 (http://mcm.york.ac.uk/browse.htt?species=APINCNO3). The inorganic reactions are shown in Table S6. The relevant rate constants for inorganic reactions were from MCM (http://mcm.york.ac.uk/parameters/simple.htt, http://mcm.york.ac.uk/parameters/photolysis_param.htt, and http://mcm.york.ac.uk/parameters/complex.htt).

Table S6. The inorganic reactions included in model simulations:

Reactions	Rate constants[a]
$O = O_3$	5.6E-34*N_2*(TEMP/300)^-2.6*O_2+6.0E-34*O_2*(TEMP/300)^-2.6*O_2
$O + O_3 =$	8.0E-12*EXP(-2060/TEMP)
$O + NO = NO_2$	KMT01
$O + NO_2 = NO$	5.5E-12*EXP(188/TEMP)
$O + NO_2 = NO_3$	KMT02
$O_1D = O$	3.2E-11*EXP(67/TEMP)*O_2+2.0E-11*EXP(130/TEMP)*N_2
$NO + O_3 = NO_2$	1.4E-12*EXP(-1310/TEMP)
$NO_2 + O_3 = NO_3$	1.4E-13*EXP(-2470/TEMP)
$NO + NO = NO_2 + NO_2$	3.3E-39*EXP(530/TEMP)*O_2
$NO + NO_3 = NO_2 + NO_2$	1.8E-11*EXP(110/TEMP)
$NO_2 + NO_3 = NO + NO_2$	4.50E-14*EXP(-1260/TEMP)
$NO_2 + NO_3 = N_2O_5$	KMT03
$O_1D = OH + OH$	2.14E-10*H_2O
$OH + O_3 = HO_2$	1.70E-12*EXP(-940/TEMP)
$OH + H_2 = HO_2$	7.7E-12*EXP(-2100/TEMP)
$OH + CO = HO_2$	KMT05
$OH + H_2O_2 = HO_2$	2.9E-12*EXP(-160/TEMP)
$HO_2 + O_3 = OH$	2.03E-16*(TEMP/300)^4.57*EXP(693/TEMP)
$OH + HO_2 =$	4.8E-11*EXP(250/TEMP)
$HO_2 + HO_2 = H_2O_2$	2.20E-13*KMT06*EXP(600/TEMP)+1.90E-33*M*KMT06*EXP(980/TEMP)
$OH + NO = HONO$	KMT07
$OH + NO_2 = HNO_3$	KMT08
$OH + NO_3 = HO_2 + NO_2$	2.00E-11
$HO_2 + NO = OH + NO_2$	3.45E-12*EXP(270/TEMP)
$HO_2 + NO_2 = HO_2NO_2$	KMT09
$OH + HO_2NO_2 = NO_2$	3.2E-13*EXP(690/TEMP)*1.0
$HO_2 + NO_3 = OH + NO_2$	4.00E-12
$OH + HONO = NO_2$	2.5E-12*EXP(260/TEMP)
$OH + HNO_3 = NO_3$	KMT11
$O_3 = O_1D$	Jvalue[1]
$O_3 = O$	Jvalue[2]
$H_2O_2 = OH + OH$	Jvalue[3]
$NO_2 = NO + O$	Jvalue[4]
$NO_3 = NO$	Jvalue[5]
$NO_3 = NO_2 + O$	Jvalue[6]
$HONO = OH + NO$	Jvalue[7]
$HNO_3 = OH + NO_2$	Jvalue[8]
$N_2O_5 = NO_2 + NO_3$	KMT04
$HO_2NO_2 = HO_2 + NO_2$	KMT10

[a.] The unit of first-order rate constant is s^{-1} and the unit of second-order rate constant is cm^3 $molec^{-1}$ s^{-1}.

5.3 Model simulation under chamber conditions

5.3.1 Background experiment

For background experiment, we turned on the lights for 4 h without adding any chemical to the chamber and recorded the formation trend for O_3. The average NO concentration was 0.31 ppbv, which is lower than the detection limit of NO monitor (0.4 ppbv).
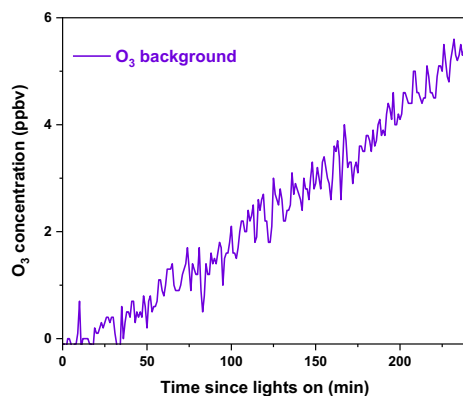
Figure S12. Time series of NO and O_3 from background experiment during irradiation.

5.3.2 Chamber simulation results

The following conditions were used as input parameters:

1. Initial concentrations: 3°_ApHN = 6.3 ppbv, NO = 0 or 1 ppbv, NO_2 = 0 ppbv, and OH = 5.8×10^5 molecule/cm^3;

2. O_3 source = 0.02 ppbv/min;

3. Temperature = 295 K; Relative humidity: RH = 0%;

4. OH reaction rate constant for 3°_ApHN = 9.9×10^{-10} cm^3 molecule^{-1} s^{-1} (estimated by MCM); NO_3 radical reaction rate constant for 3°_ApHN = 7.2×10^{-12} cm^3 molecule^{-1} s^{-1} (estimated by MCM); ozonolysis rate constant for 3°_ApHN = 4.2×10^{-17} cm^3 molecule^{-1} s^{-1} (estimated by separate ozonolysis experiment);

5. Photolysis for all related species: The intensity of the spectral photon fluxes in the GTEC chamber was determined by measuring the lights spectra with a spectroradiometer. Through integrating the previously reported absorption cross sections and quantum yields (MCM, http://mcm.york.ac.uk/parameters/photolysis_param.htt) for all related species under our chamber light spectra.
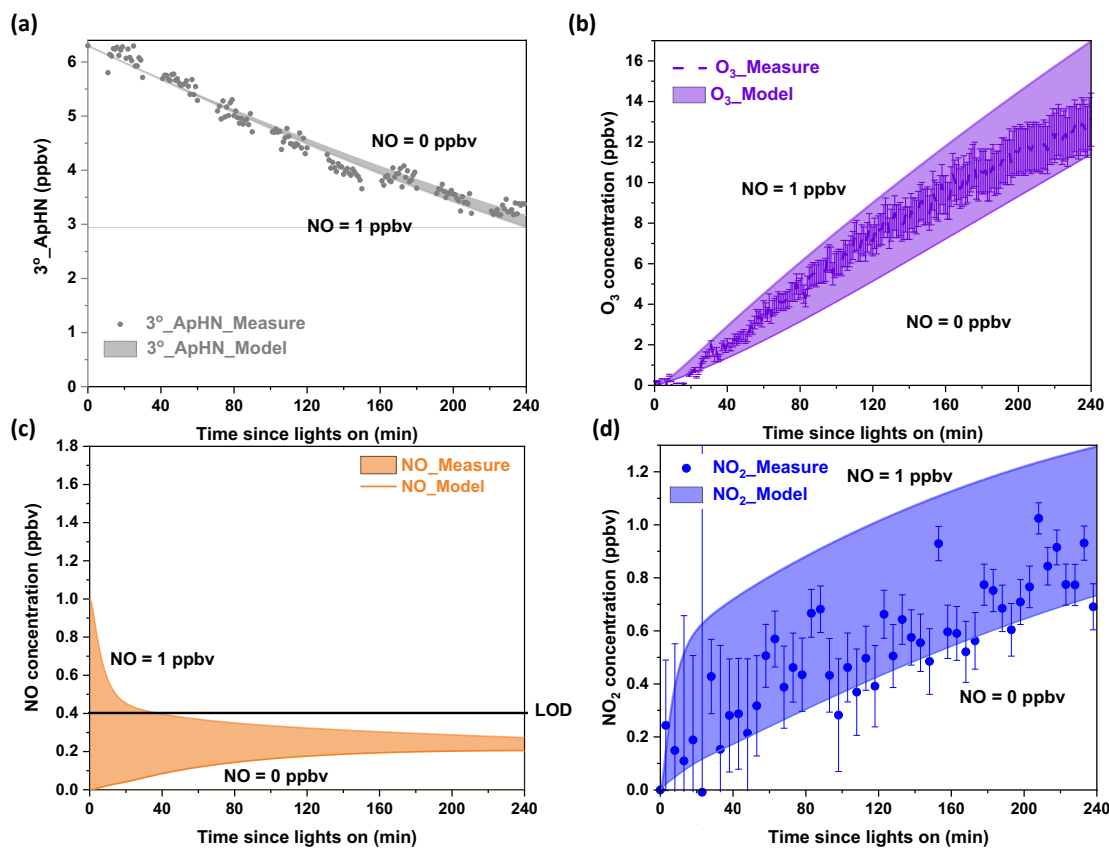
Figure S13. Model simulations with an initial NO of 0 versus 1 ppbv and experimental measurements of (a) 3°_ApHN (uncertainty of 3°_ApHN measured by the HR-ToF-CIMS was not determined, therefore there was no error bar in 3°_ApHN measurement); (b) O_3 (±10% is the uncertainty for O_3 monitor); (c) NO (NO_x monitor detection limit = 0.4 ppbv, ±4% is the uncertainty for NO_x monitor); (d) NO_2 (0.06 ppbv is the uncertainty for CAPS monitor).[32] The uncertainties of O_3 monitor and NO_x monitor are from the instrument manuals.

5.4 Model simulations of 3°_ApHN photolysis only

The following conditions were used as input parameters:

1. Initial concentrations: 3°_ApHN = 28 pptv (This concentration was roughly determined based on the reported daily average α-pinene concentration (0.37 ppbv in Atlanta, GA)[33] and the yield to produce 3°_ApHN from OH-initiated photooxidation of α-pinene (upper bound as 7.5%, which is the yield of ring-opened RO_2 which can further react with NO to produce 3°_ApHN, MCM)), NO = 0 ppbv, NO_2 = 0 ppbv (Assume 3°_ApHN was the only nitrogen source), O_3 = 46 ppbv (extracted from https://www.epa.gov/outdoor-air-quality-data/download-daily-data, average O_3 concentration in summer Atlanta, 2017), OH = 1.5×10^6 molecule/cm^3.

2. Temperature: = 298 K;

3. Relative humidity: RH = 60%

4. Solar zenith angle: 44.25°, the MCM built-in function was employed to normalize photolysis rate constants for all related species.

5. $J_{ambient}$ of 3°_ApHN under average daytime solar spectral photon fluxes and wavelength-dependent quantum yield (cutoff wavelength = 330 nm, Figure S14) = 10.2×10^{-5} s^{-1}.
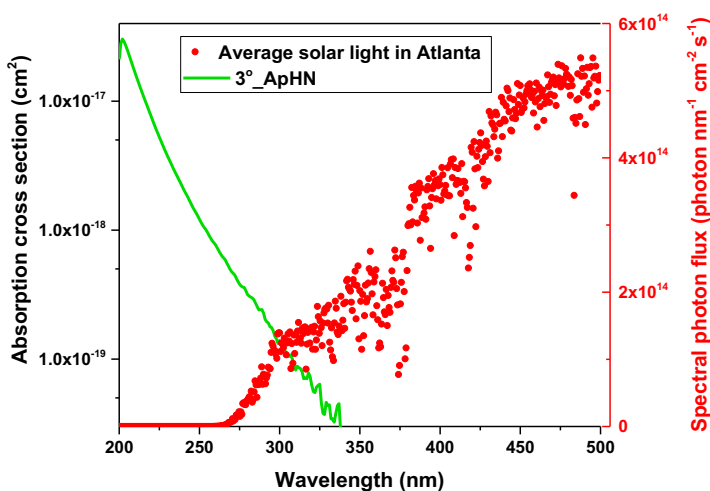
Figure S14. Absorption cross section for 3°_ApHN and average daytime solar spectral photon flux on August 1 from 7:00 am to 7:00 pm (Eastern time, solar spectra extracted from TUV-radiation model, August 1 at 33.75° latitude north (Atlanta), overhead ozone column 300 Du, and albedo 0.1).

References:

(1)   Barnes, I.; Becker, K. H.; Zhu, T. Near UV Absorption Spectra and Photolysis Products of
       Difunctional Organic Nitrates: Possible Importance as NOx Reservoirs. *J. Atmos. Chem.* **1993**, *17*
       (4), 353–373. https://doi.org/10.1007/BF00696854.

(2)   Treves, K.; Rudich, Y. The Atmospheric Fate of C3-C6 Hydroxyalkyl Nitrates. *J. Phys. Chem. A*
       2003, *107* (39), 7809–7817. https://doi.org/10.1021/jp035064l.

(3)   Suarez-Bertoa, R.; Picquet-Varrault, B.; Tamas, W.; Pangui, E.; Doussin, J. F. Atmospheric Fate
       of a Series of Carbonyl Nitrates: Photolysis Frequencies and OH-Oxidation Rate Constants.
       Environ. Sci. Technol. **2012**, *46* (22), 12502–12509. https://doi.org/10.1021/es302613x.

(4)   Müller, J. F.; Peeters, J.; Stavrakou, T. Fast Photolysis of Carbonyl Nitrates from Isoprene. *Atmos.*
       Chem. Phys. **2014**, *14* (5), 2497–2508. https://doi.org/10.5194/acp-14-2497-2014.

(5)   Xiong, F.; Borca, C. H.; Slipchenko, L. V.; Shepson, P. B. Photochemical Degradation of
       Isoprene-Derived 4,1-Nitrooxy Enal. *Atmos. Chem. Phys.* **2016**, *16* (9), 5595–5610.
       https://doi.org/10.5194/acp-16-5595-2016.

(6)   Picquet-Varrault, B.; Suarez-Bertoa, R.; Duncianu, M.; Cazaunau, M.; Pangui, E.; David, M.;
       Doussin, J. F. Photolysis and Oxidation by OH Radicals of Two Carbonyl Nitrates: 4-Nitrooxy-2-
       Butanone and 5-Nitrooxy-2-Pentanone. *Atmos. Chem. Phys.* **2020**, *20* (1), 487–498.
       https://doi.org/10.5194/acp-20-487-2020.

(7)   Roberts, J. M.; Fajer, R. W. UV Absorption Cross Sections of Organic Nitrates of Potential
       Atmospheric Importance and Estimation of Atmospheric Lifetimes. *Environ. Sci. Technol.* **1989**,
       23 (8), 945–951.

(8)   Huang, Y.; Zhao, R.; Charan, S. M.; Kenseth, C. M.; Zhang, X.; Seinfeld, J. H. Unified Theory of
       Vapor-Wall Mass Transport in Teflon-Walled Environmental Chambers. *Environ. Sci. Technol.*
       2018, *52* (4), 2134–2142. https://doi.org/10.1021/acs.est.7b05575.

(9)   McMurry, P. H.; Grosjean, D. Gas and Aerosol Wall Losses in Teflon Film Smog Chambers.
       Environ. Sci. Technol. **1985**, *19* (12), 1176–1182. https://doi.org/10.1021/es00142a006.

(10)   Grosjean, D. Wall Loss of Gaseous Pollutants in Outdoor Teflon Chambers. *Environ. Sci. Technol.*
       1985, *19* (11), 1059–1065. https://doi.org/10.1021/es00141a006.

(11)   Matsunaga, A.; Ziemann, P. J. Gas-Wall Partitioning of Organic Compounds in a Teflon Film
       Chamber and Potential Effects on Reaction Product and Aerosol Yield Measurements. *Aerosol Sci.*
       Technol. **2010**, *44* (10), 881–892. https://doi.org/10.1080/02786826.2010.501044.

(12)   Yeh, G. K.; Ziemann, P. J. Gas-Wall Partitioning of Oxygenated Organic Compounds:
       Measurements, Structure-Activity Relationships, and Correlation with Gas Chromatographic
       Retention Factor. *Aerosol Sci. Technol.* **2015**, *49* (9), 727–738.
       https://doi.org/10.1080/02786826.2015.1068427.

(13)   La, Y. S.; Camredon, M.; Ziemann, P. J.; Valorso, R.; Matsunaga, A.; Lannuque, V.; Lee-Taylor,
       J.; Hodzic, A.; Madronich, S.; Aumont, B. Impact of Chamber Wall Loss of Gaseous Organic
       Compounds on Secondary Organic Aerosol Formation: Explicit Modeling of SOA Formation from
       Alkane and Alkene Oxidation. *Atmos. Chem. Phys.* **2016**, *16* (3), 1417–1431.
       https://doi.org/10.5194/acp-16-1417-2016.

(14)   Zhang, X.; Schwantes, R. H.; McVay, R. C.; Lignell, H.; Coggon, M. M.; Flagan, R. C.; Seinfeld,
       J. H. Vapor Wall Deposition in Teflon Chambers. *Atmos. Chem. Phys.* **2015**, *15* (8), 4197–4214.
       https://doi.org/10.5194/acp-15-4197-2015.

(15)   Zhang, X.; Cappa, C. D.; Jathar, S. H.; McVay, R. C.; Ensberg, J. J.; Kleeman, M. J.; Seinfeld, J.
       H. Influence of Vapor Wall Loss in Laboratory Chambers on Yields of Secondary Organic
       Aerosol. *Proc. Natl. Acad. Sci. U. S. A.* **2014**, *111* (16), 5802–5807.
       https://doi.org/10.1073/pnas.1404727111.

(16)   Nah, T.; Mcvay, R. C.; Zhang, X.; Boyd, C. M.; Seinfeld, J. H.; Ng, N. L. Influence of Seed
       Aerosol Surface Area and Oxidation Rate on Vapor Wall Deposition and SOA Mass Yields : A
       Case Study with α -Pinene Ozonolysis. *Atmos. Chem. Phys.* **2016**, *16*, 9361–9379.
       https://doi.org/10.5194/acp-16-9361-2016.

(17)   Krechmer, J. E.; Pagonis, D.; Ziemann, P. J.; Jimenez, J. L. Quantification of Gas-Wall

Partitioning in Teflon Environmental Chambers Using Rapid Bursts of Low-Volatility Oxidized Species Generated in Situ. *Environ. Sci. Technol.* **2016**, *50* (11), 5757–5765. https://doi.org/10.1021/acs.est.6b00606.

(18)   Compernolle, S.; Ceulemans, K.; Müller, J. F. Evaporation: A New Vapour Pressure Estimation Methodfor Organic Molecules Including Non-Additivity and Intramolecular Interactions. *Atmos. Chem. Phys.* **2011**, *11* (18), 9431–9450. https://doi.org/10.5194/acp-11-9431-2011.

(19)   Shiraiwa, M.; Yee, L. D.; Schilling, K. A.; Loza, C. L.; Craven, J. S.; Zuend, A.; Ziemann, P. J.; Seinfeld, J. H. Size Distribution Dynamics Reveal Particle-Phase Chemistry in Organic Aerosol Formation. *Proc. Natl. Acad. Sci. U. S. A.* **2013**, *110* (29), 11746–11750. https://doi.org/10.1073/pnas.1307501110.

(20)   Praske, E.; Crounse, J. D.; Bates, K. H.; Kurtén, T.; Kjaergaard, H. G.; Wennberg, P. O. Atmospheric Fate of Methyl Vinyl Ketone: Peroxy Radical Reactions with NO and HO2. *J. Phys. Chem. A* **2015**, *119* (19), 4562–4572. https://doi.org/10.1021/jp5107058.

(21)   Schwantes, R. H.; Teng, A. P.; Nguyen, T. B.; Coggon, M. M.; Crounse, J. D.; St. Clair, J. M.; Zhang, X.; Schilling, K. A.; Seinfeld, J. H.; Wennberg, P. O. Isoprene NO3 Oxidation Products from the RO2 + HO2 Pathway. *J. Phys. Chem. A* **2015**, *119* (40), 10158–10171. https://doi.org/10.1021/acs.jpca.5b06355.

(22)   St. Clair, J. M.; Rivera-Rios, J. C.; Crounse, J. D.; Knap, H. C.; Bates, K. H.; Teng, A. P.; Jorgensen, S.; Kjaergaard, H. G.; Keutsch, F. N.; Wennberg, P. O. Kinetics and Products of the Reaction of the First-Generation Isoprene Hydroxy Hydroperoxide (ISOPOOH) with OH. *J. Phys. Chem. A* **2016**, *120* (9), 1441–1451. https://doi.org/10.1021/acs.jpca.5b06532.

(23)   Schwantes, R. H.; Schilling, K. A.; McVay, R. C.; Lignell, H.; Coggon, M. M.; Zhang, X.; Wennberg, P. O.; Seinfeld, J. H. Formation of Highly Oxygenated Low-Volatility Products from Cresol Oxidation. *Atmos. Chem. Phys.* **2017**, *17* (5), 3453–3474. https://doi.org/10.5194/acp-17-3453-2017.

(24)   Bates, K. H.; Crounse, J. D.; St. Clair, J. M.; Bennett, N. B.; Nguyen, T. B.; Seinfeld, J. H.; Stoltz, B. M.; Wennberg, P. O. Gas Phase Production and Loss of Isoprene Epoxydiols. *J. Phys. Chem. A* **2014**, *118* (7), 1237–1246. https://doi.org/10.1021/jp4107958.

(25)   Loza, C. L.; Craven, J. S.; Yee, L. D.; Coggon, M. M.; Schwantes, R. H.; Shiraiwa, M.; Zhang, X.; Schilling, K. A.; Ng, N. L.; Canagaratna, M. R. et al. Secondary Organic Aerosol Yields of 12-Carbon Alkanes. *Atmos. Chem. Phys.* **2014**, *14* (3), 1423–1439. https://doi.org/10.5194/acp-14-1423-2014.

(26)   Loza, C. L.; Chan, A. W. H.; Galloway, M. M.; Keutsch, F. N.; Flagan, R. C.; Seinfeld, J. H. Characterization of Vapor Wall Loss in Laboratory Chambers. *Environ. Sci. Technol.* **2010**, *44* (13), 5074–5078. https://doi.org/10.1021/es100727v.

(27)   Vereecken, L.; Peeters, J. Decomposition of Substituted Alkoxy Radicals - Part I: A Generalized Structure-Activity Relationship for Reaction Barrier Heights. *Phys. Chem. Chem. Phys.* **2009**, *11* (40), 9062–9074. https://doi.org/10.1039/b909712k.

(28)   Vereecken, L.; Peeters, J. A Structure-Activity Relationship for the Rate Coefficient of H-Migration in Substituted Alkoxy Radicals. *Phys. Chem. Chem. Phys.* **2010**, *12* (39), 12608–12620. https://doi.org/10.1039/c0cp00387e.

(29)   Skoog, D. A.; West, D. M.; Holler, F. J.; Crouch, S. R. *Fundamentals of Analytical Chemistry, 9th Edition*; Boston, 2014.

(30)   Jenkin, M. E.; Saunders, S. M.; Wagner, V.; Pilling, M. J. Protocol for the Development of the Master Chemical Mechanism, MCM v3 (Part B): Tropospheric Degradation of Aromatic Volatile Organic Compounds. *Atmos. Chem. Phys.* **2003**, *3* (1), 181–193. https://doi.org/10.5194/acp-3-181-2003.

(31)   Jenkin, M. E.; Saunders, S. M.; Pilling, M. J. The Tropospheric Degradation of Volatile Organic Compounds: A Protocol for Mechanism Development. *Atmos. Environ.* **1997**, *31* (1), 81–104. https://doi.org/10.1016/S1352-2310(96)00105-7.

(32)   Kebabian, P. L.; Wood, E. C.; Herndon, S. C.; Freedman, A. An Alternative Approach to Monitoring Nitrogen Dioxide: Cavity Attenuated Phase Shift Spectroscopy. *Air Waste Manag. Assoc. Symp. Air Qual. Meas. Methods Technol. 2008* **2008**, *42* (16), 214–218.

(33)   Chen, Y.; Takeuchi, M.; Nah, T.; Xu, L.; Canagaratna, M. R.; Stark, H.; Baumann, K.; Canonaco,

F.; Prevot, A. S. H.; Gregory Huey, L. et al. Chemical Characterization of Secondary Organic Aerosol at a Rural Site in the Southeastern US: Insights from Simultaneous High-Resolution Time-of-Flight Aerosol Mass Spectrometer (HR-ToF-AMS) and FIGAERO Chemical Ionization Mass Spectrometer (CIMS) Measur. *Atmos. Chem. Phys.* **2020**, *20* (14), 8421–8440. https://doi.org/10.5194/acp-20-8421-2020.